

The Composition Of A Disrupted Extrasolar Planetesimal At SDSS J0845+2257 (Ton 345)

D. J. Wilson^{1*}, B. T. Gänsicke¹, D. Koester², O. Toloza¹, A. F. Pala¹,
E. Breedt¹, S. G. Parsons³

¹ *Department of Physics, University of Warwick, Coventry CV4 7AL, UK*

² *Institut für Theoretische Physik und Astrophysik, University of Kiel, 24098 Kiel, Germany*

⁴ *Departamento de Física y Astronomía, Universidad de Valparaíso, Avenida Gran Bretaña 1111, Valparaíso 2360102, Chile*

Accepted 2015 May 22. Received 2015 May 22; in original form 2015 February 20

ABSTRACT

We present a detailed study of the metal-polluted DB white dwarf SDSS J0845+2257 (Ton 345). Using high-resolution *HST*/COS and VLT spectroscopy, we have detected hydrogen and eleven metals in the atmosphere of the white dwarf. The origin of these metals is almost certainly the circumstellar disc of dusty and gaseous debris from a tidally-disrupted planetesimal, accreting at a rate of $1.6 \times 10^{10} \text{ g s}^{-1}$. Studying the chemical abundances of the accreted material demonstrates that the planetesimal had a composition similar to the Earth, dominated by rocky silicates and metallic iron, with a low water content. The mass of metals within the convection zone of the white dwarf corresponds to an asteroid of at least $\sim 130\text{--}170 \text{ km}$ in diameter, although the presence of ongoing accretion from the debris disc implies that the planetesimal was probably larger than this. While a previous abundance study of the accreted material has shown an anomalously high mass fraction of carbon (15 percent) compared to the bulk Earth, our independent analysis results in a carbon abundance of just 2.5 percent. Enhanced abundances of core material (Fe, Ni) suggest that the accreted object may have lost a portion of its mantle, possibly due to stellar wind stripping in the asymptotic giant branch. Time-series spectroscopy reveals variable emission from the orbiting gaseous disc, demonstrating that the evolved planetary system at SDSS J0845+2257 is dynamically active.

Key words: white dwarfs - stars: individual: SDSS J0845+2257 - planets and satellites: composition - planetary systems

1 INTRODUCTION

Since the discovery of calcium absorption lines in the atmosphere of van Maanen 2 (van Maanen 1917; Weidemann 1960), an explanation has been sought for the metal pollution observed in many white dwarfs. The high surface gravity ($\log g$) of white dwarfs implies that all metals will sink out of their atmospheres on time-scales that are short relative to the cooling age, leaving pristine hydrogen or helium atmospheres. However, metal pollution is now thought to be present at 25–50 percent of all white dwarfs (Zuckerman et al. 2003, 2010; Koester et al. 2014a; Barstow et al. 2014). Whilst radiative levitation can explain the observed metals in some white dwarfs with effective temperatures (T_{eff}) above 20000 K (Chayer et al. 1995;

Chayer 2014; Koester et al. 2014a), metal-polluted white dwarfs cooler than this must be currently accreting, or have recently accreted, material from an external source (Koester 2009).

Historically the source of this accretion was thought to be the interstellar medium (Aannestad & Sion 1985; Sion et al. 1988). The explanation that is now generally accepted developed from the infrared detection of a dusty debris disc, formed by the tidal disruption of an asteroid, around the white dwarf G29-38 (Zuckerman & Becklin 1987; Graham et al. 1990; Jura 2003). Since then more than 30 similar discs have been discovered, and current estimates suggest that 1–3 percent of white dwarfs possess detectable dusty debris disks (Farihi et al. 2009; Girven et al. 2011; Steele et al. 2011; Barber et al. 2014; Rocchetto et al. 2014). Debris from these disrupted planetesimals accreting on the white dwarfs is now thought to be the dominant

* d.j.wilson.1@warwick.ac.uk

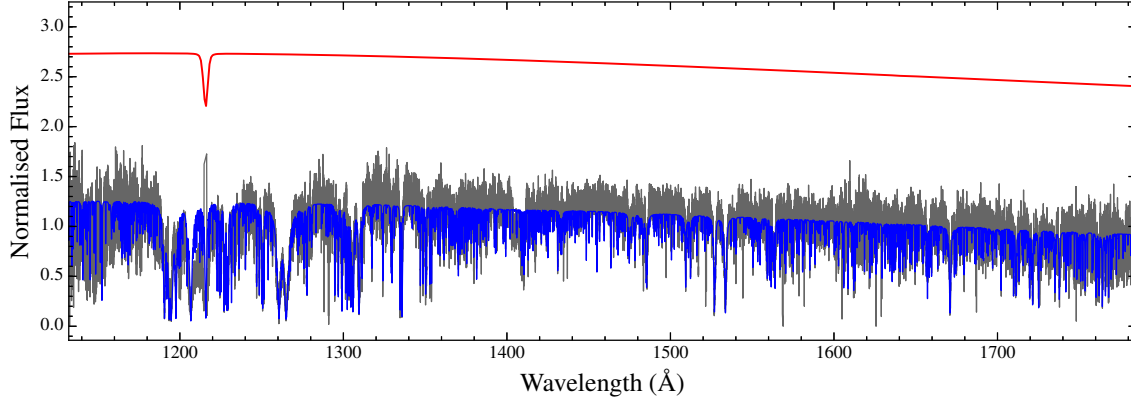


Figure 1. *HST*/COS FUV spectrum of SDSS J0845+2257 obtained on 2010 April 01 (grey), with the model fit used to determine the abundances of the accreted metals (blue). Plotted in red is a model spectrum for a white dwarf with the same atmospheric parameters, but no metals. The extremely large number of metal absorption lines in the spectrum of SDSS J0845+2257 is successfully reproduced by the model fit, with the exception of the two sections shown in Figure 4.

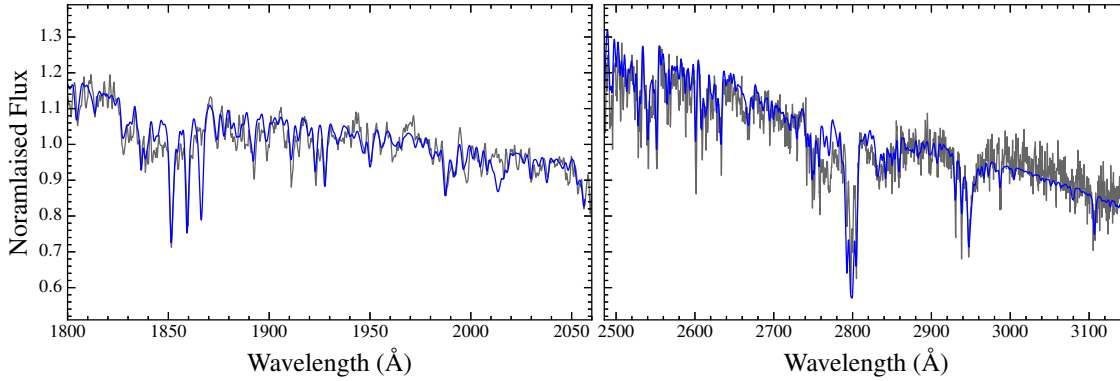


Figure 2. *HST*/COS NUV spectrum of SDSS J0845+2257 obtained on 2010 March 31 (grey), with the model fit used to determine the abundances of the accreted metals (blue). The model under-predicts the Mg II 2790 Å triplet, possibly due to emission from the gaseous debris disc (§ 5).

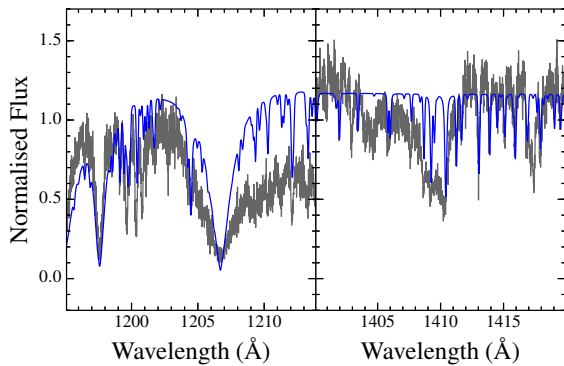


Figure 4. The model fit to the FUV spectrum under-predicts the red wing of the 1206 Å Si III resonance line and what appear to be Si lines around 1400 Å. The reason for the poor fit in these areas is unknown, but a similar feature is seen in GALEX 1931+0117 (see fig. 4 in Gänsicke et al. 2012).

source of the atmospheric metals. In summary, these discoveries reveal the presence of evolved planetary systems at white dwarfs, offering an insight into the end-stages of planetary evolution. Zuckerman (2014) noted that, in hindsight,

the discovery of van Maanen 2 was therefore the first observational evidence of an extrasolar planetary system.

In most white dwarfs pollution from only one or two elements, usually Ca and/or Mg, has been detected. However high-resolution spectroscopy of an increasing number of systems has revealed pollution by large number of metals, with a record of 16 species detected in the case of GD 362 (Xu et al. 2013). Around a dozen white dwarfs show photospheric O, Mg, Si and Fe (Gänsicke et al. 2012; Dufour et al. 2012; Klein et al. 2011; Jura et al. 2012; Farihi et al. 2013; Xu et al. 2014; Raddi et al. 2015). These four elements make up >90% of the bulk Earth (Allègre et al. 2001).

Consequently these systems provide a unique opportunity to study the bulk chemical composition of extrasolar planetary systems. Thus far, two main conclusions have been reached: 1. To zeroth order the chemical composition of the accreted debris is similar to that of the terrestrial planets in the Solar System (Zuckerman et al. 2007; Jura & Young 2014), with a distinct lack of volatile elements (Jura 2006; Farihi et al. 2009); 2. Within this overall similarity there is a large amount of diversity, with some systems showing evidence of differentiation (Gänsicke et al. 2012), post-nebula processing (Xu et al. 2013) and water-rich asteroids (Farihi et al. 2013; Raddi et al. 2015).

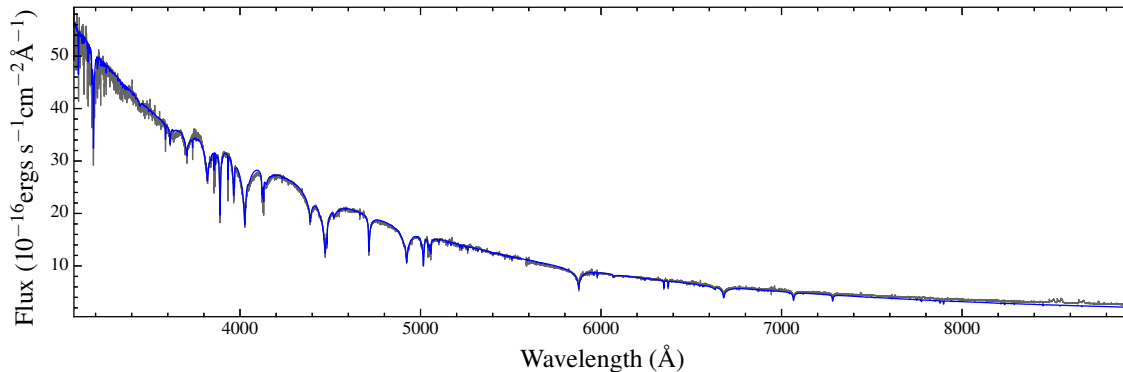


Figure 3. Full optical spectrum of SDSS J0845+2257 from the UVB and VIS arms of X-shooter (grey) together with the model fit (blue) used to calculate the atmospheric parameters and the metal abundances. A telluric correction was applied using the X-shooter spectral library (Chen et al. 2014). The model is over-plotted using just one scaling factor for the entire spectrum, demonstrating the excellent flux calibration of the X-shooter data.

We present ultraviolet and times-series optical spectra of the metal-polluted DB white dwarf SDSS J084539.17+225728.0 (henceforth SDSS J0845+2257). This object was originally classified as a sdO subdwarf, Ton 345 (Green et al. 1986). As part of a search for Ca II 8600 Å emission lines among white dwarfs with SDSS spectra, Gänsicke et al. (2008) found that SDSS J0845+2257 was in fact a DB (helium atmosphere) white dwarf with a gaseous disc. Follow-up observations obtained with the William Herschel Telescope (WHT) revealed a significant change in the shape and strength of the Ca II 8600 Å emission line profile, along with strong photospheric absorption lines from Ca, Si and Mg.

Jura et al. (2015) presented a Keck/HIRES study detecting 11 metals in the atmosphere of SDSS J0845+2257. We extend these observations into the ultraviolet and carry out an independent detailed study of the accreted material. We also present updated time-series observations of variable emission from the gaseous disc around SDSS J0845+2257 and an analysis of the *HST*/COS high-speed ultraviolet photometry.

2 OBSERVATIONS

Since the publication of Gänsicke et al. (2008) we have obtained deep spectroscopic observations of SDSS J0845+2257 in the ultraviolet with the *Hubble Space Telescope* (*HST*) and in the optical with the ESO Very Large Telescope (VLT) and Gemini South. Table 1 provides a log of our observations.

HST observed SDSS J0845+2257 on 2010 March 31 and 2010 April 01 with the Cosmic Origins Spectrograph (COS, Green et al. 2012). Eight orbits were awarded under proposal ID 11561 for a total exposure time of 2735 s, 4994 s and 14397 s with the G130M, G160M and G230L gratings respectively. The spectra were processed with CALCOS 2.12. Both the FUV (1120–1800 Å, Figure 1) and NUV (1600–2060 Å, 2470–3150 Å, Figure 2) spectra show a host of metal absorption lines, with only small amounts of continuum remaining.

Optical observations of SDSS J0845+2257 were obtained at the VLT on 2008 April 03–05, 2009 January 08 and 2009 April 09–11 with the Ultraviolet and Visual

Echelle Spectrograph (UVES, Dekker et al. 2000) and again on 2011 January 29 and 2014 October 20 with X-shooter (Vernet et al. 2011). Total exposure times were 47520 s with UVES and 10721 s with X-shooter. These observations were reduced using the standard procedures within the REFLEX¹ reduction tool developed by ESO. A heliocentric correction was applied to the REFLEX outputs, and multiple exposures from the same night were combined. The optical spectra show a large number of absorption lines, indicative of pollution from a variety of metals. The 8600 Å Ca II emission line triplet is also clearly visible in all of the observations (see § 5).

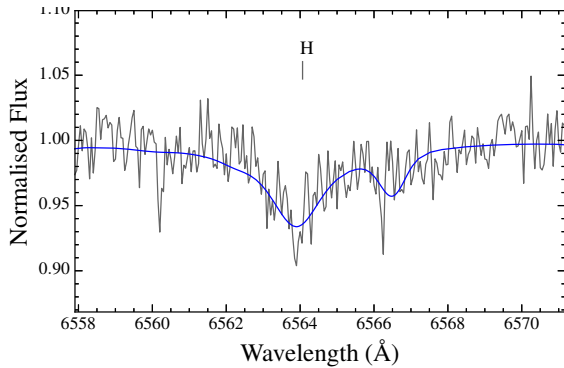
On 2010 April 02 we obtained six spectra of SDSS J0845+2257 using the Gemini Multi-object Spectrograph on Gemini South (GMOS, Hook et al. 2004). The observations were made in service mode, using the R831 grating and a 1'' slit, which gave a wavelength range of 7540–9665 Å at a resolution of 2.0 Å. We requested the acquisition to be done in the *i* band to ensure that the target was properly centred on the slit in the region of the Ca II lines. We reduced and extracted the spectra using the STARLINK software packages KAPPA and PAMELA, and then applied the wavelength and flux calibration using MOLLY². The wavelength calibration was derived from a CuAr arc exposure taken in the morning following the observations and adjusted according to the known wavelengths of strong night sky emission lines. The flux calibration was calculated using an observation of the spectroscopic standard star LTT3218. Finally, we combined the six individual exposures to give a single, high signal-to-noise spectrum with a combined exposure time of 4980 s. The strength of the 8600 Å Ca II triplet in this spectrum is comparable to the other optical observations.

¹ The REFLEX software and documentation can be obtained from <http://www.eso.org/sci/software/reflex/>

² MOLLY was written by T.R. Marsh and is available from <http://www.warwick.ac.uk/go/trmarsh/software/>.

Table 1. Log of observations of SDSS J0845+2257

Date	Telescope/ Instrument	Wavelength Range (Å)	Spectral Resolution (Å)	Total Exposure Time (s)
2004 December 19	SDSS	3794–9199	0.9–2.1	3300
2008 January 02	WHT/ISIS	3577–8840	1.0–2.0	2400
2008 April 03–5	VLT/UVES	3280–9460	0.02	17820
2008 January 08	VLT/UVES	3280–9460	0.02	11880
2009 April 09–11	VLT/UVES	3280–9460	0.02	17820
2010 March 31	<i>HST</i> /COS	2470–3150	0.01	7727
2010 April 01	<i>HST</i> /COS	1600–3150	0.39	14397
2010 April 02	Gemini South/GMOS	7540–9665	2.0	4980
2011 January 29	VLT/X-shooter	2990–24790	0.2–0.6	6990
2014 October 20	VLT/X-shooter	2990–24790	0.2–0.6	3731

**Figure 5.** Section of our UVES spectrum showing a weak H α absorption line. Fitting an atmospheric model (blue) to the spectrum results in $\log(\text{H}/\text{He}) = -5.10 \pm 0.50$.

3 WHITE DWARF PARAMETERS

The spectroscopic determination of atmospheric parameters for hot DB white dwarfs is extremely difficult, because the spectra hardly change between $T_{\text{eff}} = 20000\text{--}30000$ K. Using a fit to the SDSS photometry with a fixed $\log g = 8.00$, we obtain $T_{\text{eff}} = 19850 \pm 600$ K for a pure He grid, $T_{\text{eff}} = 19890 \pm 620$ K for a grid with $\log(\text{H}/\text{He}) = -5.0$, and $T_{\text{eff}} = 19880 \pm 600$ K for a grid with our final metal abundances. The increase of the free electron density, which is the major effect from the inclusion of metals in cooler DB models, has no significant effect at these temperatures. There is, however, a noticeable blanketing effect from the strong metal lines in the ultraviolet. This increases the overall flux in the optical range, but with the same factor in all SDSS band passes. It therefore has no effect on the atmospheric parameter determination.

A possible difficulty when using the photometry for faint and distant objects is the interstellar reddening. The maximum reddening in the direction of SDSS J0845+2257 is $E(B-V) = 0.0268$ (Schlafly & Finkbeiner 2011). If we apply this value and repeat the fitting with the dereddened photometry, the result is a much higher temperature of $T_{\text{eff}} = 24320 \pm 920$ K. From the solid angle obtained through this fit, and assuming a radius of the white dwarf which corresponds to $\log g = 8.0$, we can obtain the distance to the white dwarf and estimate the true reddening. We find a distance of 117 pc and a vertical distance above the galac-

tic plane of 67 pc. Using the algorithm of Tremblay et al. (2011, see also Genest-Beaulieu & Bergeron 2014), we estimate a negligible reddening of $E(B-V) = 0.001$, and thus the lower T_{eff} is secure.

The atmospheric parameters from the photometry are confirmed by a fit to the SDSS spectrum, which results in $T_{\text{eff}} = 19800 \pm 70$ K, $\log g = 8.16 \pm 0.02$ for the pure He grid, and $T_{\text{eff}} = 19780 \pm 70$ K, $\log g = 8.18 \pm 0.02$ for the grid with $\log(\text{H}/\text{He}) = -5.0$. A final test is offered by the absolute calibration of the *HST* spectra. Using the solid angle from the photometry, the effective temperature is confined to $T_{\text{eff}} = 19750 \pm 250$ K by the comparison of the predicted ultraviolet fluxes with the observations. Our final compromise for the atmospheric parameters is the spectroscopic fit with the $\log(\text{H}/\text{He}) = -5$ grid, with enlarged errors:

$$T_{\text{eff}} = 19780 \pm 250 \text{ K} \quad \log g = 8.18 \pm 0.20$$

The hydrogen abundance is consistent with a fit to the H α line found in the UVES spectrum (Figure 5).

Jura et al. (2015) rely entirely on a fit to the SDSS photometry, obtaining $T_{\text{eff}} = 19535 \pm 700$ K for a pure He grid and $T_{\text{eff}} = 18700 \pm 700$ K for a grid with the observed metal abundances. The surface gravity cannot be obtained from the photometry so they fixed $\log g = 8.00$. We have computed a model adopting the parameters of Jura et al. (2015) and multiplied it with the solid angle obtained from their photometric fit. Their lower T_{eff} under-predicts the COS ultraviolet fluxes by 15–23 percent. Whilst a temperature difference of 1000 K would not normally have a large effect on the metal abundances, in this case all elements heavier than oxygen are in a transition from first to second ionization stage so the predicted lines in our, hotter, model are significantly weaker. We thus obtain larger abundances for all elements, with the exception of carbon. Our carbon abundance is based on the COS ultraviolet spectroscopy, which contains more and stronger carbon lines than the optical data analysed by Jura et al. (2015). An independent model atmosphere analysis of the COS ultraviolet spectra of SDSS J0845+2257 carried out by P. Dufour (private communication), adopting our atmospheric parameters, confirms the low photospheric carbon abundance.

Using our results for T_{eff} and $\log g$, and the helium atmosphere models of Bergeron and collaborators³, we find

³ <http://www.astro.umontreal.ca/~bergeron/CoolingModels>,

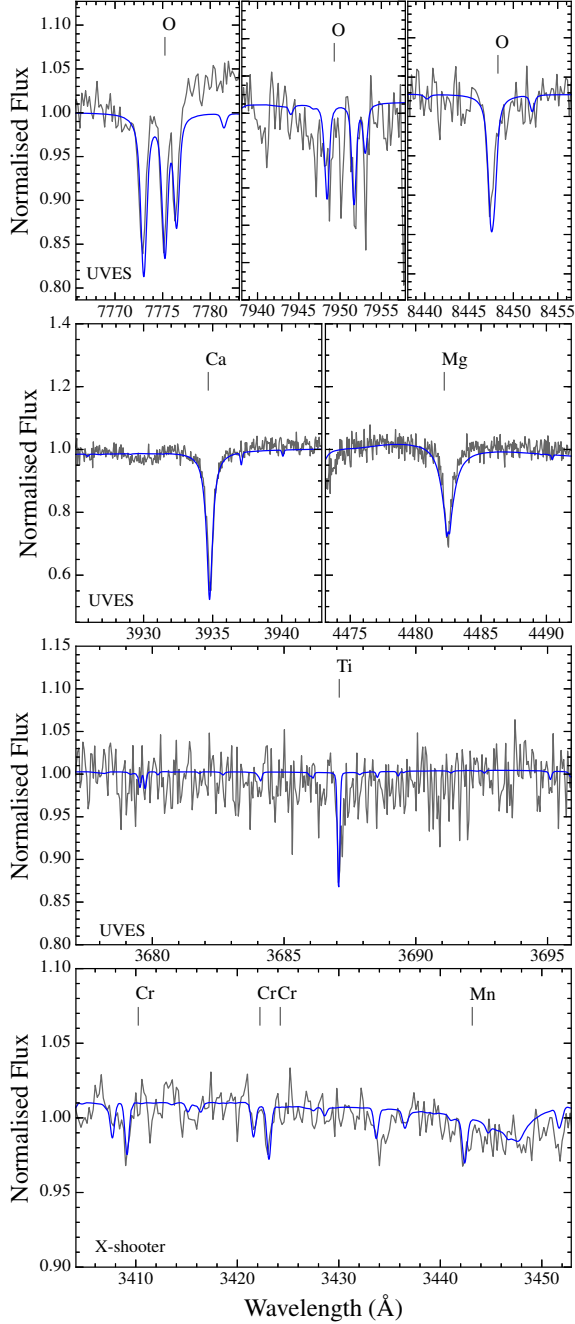


Figure 6. Normalised sections of X-Shooter and UVES spectra showing absorption lines from O, Ca, Mg, Ti, Cr and Mn, with the model atmosphere fit used to calculate the abundances over-plotted in blue. The section shown in the top-middle panel is affected by telluric lines, which are not reproduced by our model.

a cooling age $T_{\text{cool}} \approx 100$ Myr, white dwarf mass $M_{\text{wd}} = 0.679 M_{\odot}$ and radius $R_{\text{wd}} = 0.011 R_{\odot}$. Starting from a Rossland optical depth $\tau_r = 100$ and integrating the envelope equations downwards using the equation of state of Saumon et al. (1995), we find a convection zone mass of

based on Holberg & Bergeron (2006), Kowalski & Saumon (2006), Tremblay et al. (2011) and Bergeron et al. (2011).

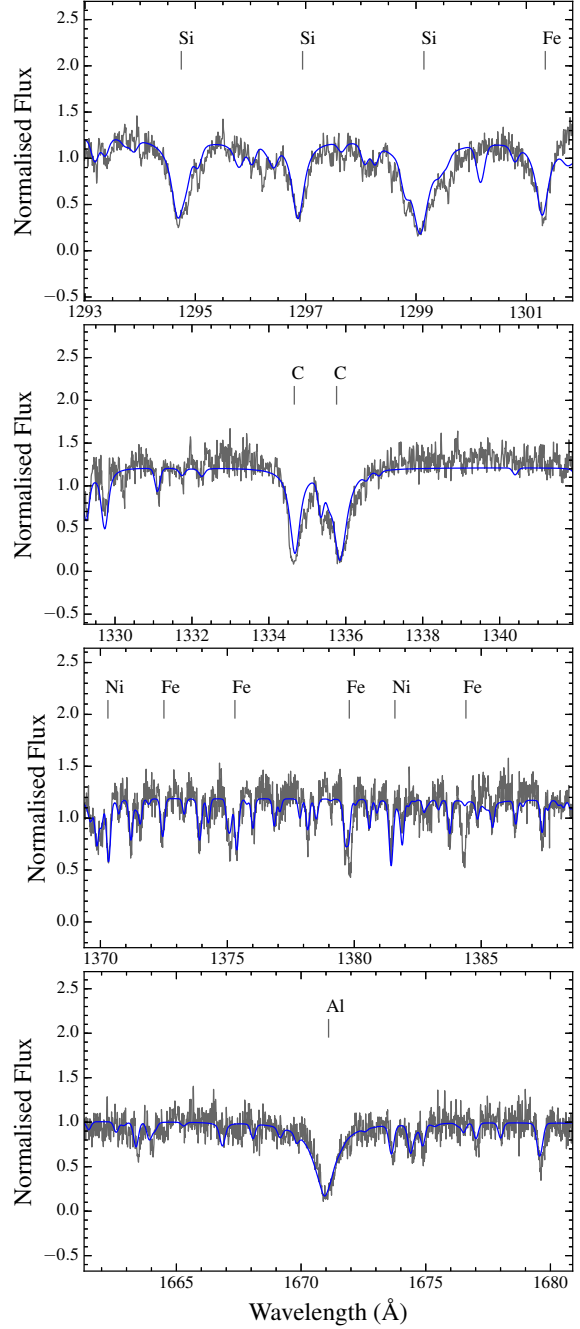


Figure 7. Sections of the COS FUV spectrum showing absorption lines from Si, C, Ni, Fe and Al, with the model atmosphere fit used to calculate the abundances over-plotted in blue.

$\log(M_{\text{cvz}}/M_{\text{wd}}) = -8.4$. Using the initial-to-final mass relationships of Gesicki et al. (2014), Casewell et al. (2009) and Catalán et al. (2008) we find a progenitor mass of $\sim 2.7 M_{\odot}$, similar to most metal-polluted white dwarfs (Jura & Xu 2012; Koester et al. 2014a) and equivalent to an A-type star progenitor.

Table 2. Measured atmospheric abundances, computed diffusion time-scales and inferred metal accretion rates in the atmosphere of SDSS J0845+2257.

Element	$\log n(Z)/n(\text{He})$	$\tau_{\text{diff}} (10^4 \text{yr})$	$\dot{M} [\text{g s}^{-1}]$
1 H	-5.10 ± 0.50	n/a	n/a
6 C	-4.90 ± 0.20	1.5	4.1×10^8
7 N	≤ -6.30	1.5	$\leq 1.9 \times 10^7$
8 O	-4.25 ± 0.20	0.97	3.8×10^9
12 Mg	-4.70 ± 0.15	1.2	1.6×10^9
13 Al	-5.70 ± 0.15	1.2	1.9×10^8
14 Si	-4.80 ± 0.30	1.2	1.5×10^9
16 S	≤ -5.40	1.2	$\leq 4.3 \times 10^8$
20 Ca	-5.95 ± 0.10	0.97	1.9×10^8
21 Sc	≤ -7.70	0.65	$\leq 5.7 \times 10^6$
22 Ti	≤ -7.15	0.59	$\leq 2.4 \times 10^7$
24 Cr	-6.40 ± 0.30	0.53	1.6×10^8
25 Mn	-7.00 ± 0.40	0.49	4.6×10^7
26 Fe	-4.60 ± 0.20	0.87	6.6×10^9
28 Ni	-5.65 ± 0.30	0.44	1.2×10^9
Total			1.6×10^{10}

Table 3. Mass fractions of the accreted debris in the convection zone of SDSS J0845+2257 and in the bulk Earth (Allègre et al. 2001). In the early-phase/instantaneous approximation the mass fractions are calculated using the atmospheric abundances, whilst in steady-state the inferred accretion rates are used. The differences between the two approximations are small for most elements.

Element	Percentage by mass		Bulk Earth
	SDSS J0845+2257 Early-Phase	Steady-State	
6 C	4.0 ± 1.8	2.5 ± 1.2	0.17
8 O	23.8 ± 11.0	23.4 ± 10.8	32.4
12 Mg	12.7 ± 4.4	9.9 ± 3.4	15.8
13 Al	1.4 ± 0.5	1.2 ± 0.4	1.5
14 Si	11.8 ± 8.1	9.3 ± 6.4	17.1
20 Ca	1.2 ± 0.3	1.2 ± 0.3	1.62
24 Cr	0.55 ± 0.38	0.99 ± 0.68	0.42
25 Mn	0.15 ± 0.13	0.28 ± 0.26	0.14
26 Fe	37.3 ± 17.1	40.8 ± 18.8	28.8
28 Ni	3.4 ± 2.4	7.5 ± 5.2	1.69
Other	3.7	2.9	1.08

4 ACCRETION OF PLANETARY MATERIAL

The ultraviolet and optical spectra (Figures 1, 2 and 3) of SDSS J0845+2257 show metal absorption lines from a variety of elements, from which we can confidently measure the atmospheric abundances for hydrogen and 10 metals and place an upper limit on 4 further metals.

The spectra show many dozens to hundreds of lines of Mg, Si, Ca and Fe, so the measured abundances for those elements are fairly secure. The Ni abundance is confirmed by the clear and moderately strong lines at 1317 Å and 1370 Å. Our carbon abundance is based on more than 15 strong C I and C II lines between 1270 Å and 1470 Å and thus also fairly robust. The O abundance relies on the 7777 Å, 7949 Å and 8448 Å lines shown in Figure 6. As with Dufour et al. (2012), we find the abundance obtained using the 7949 Å absorption line to be highly discrepant with the other two lines. As the

available atomic data for this line is limited, we have chosen to neglect this point, with the final abundance and error calculated from the remaining two lines. The 1152 Å and 1302 Å lines detected in the ultraviolet spectra allow a less precise measurement which is compatible with this result.

One of the four metals for which we only present upper limits, Ti, is actually detected in our spectra. However there is disagreement between the abundance measurements from lines at 3686 Å and 3762 Å, which fit the quoted abundance value, and the 3760 Å line, which is weaker than predicted by the model. Another line predicted by the model atmosphere, 3901 Å, is not observed. For these reasons we only feel confident to present an upper limit for the abundance of Ti.

To study the composition of the progenitor object we must compute the relative abundance ratios of the elements being accreted into the white dwarf atmosphere. These are not identical to the ratios of the photospheric metal abundances derived above, as individual metals sink out of the He envelope on different diffusion time-scales. The diffusion time-scales are a function of the depth of the convection zone and the diffusion velocity of each element, both of which vary with T_{eff} (Koester 2009).

SDSS J0845+2257 has a shallow ($\log (M_{\text{cvz}}/M_{\text{wd}}) = -8.4$) convection zone and we assume that the accreted metals are homogeneously mixed, such that the relative ratios of elements near the bottom of the convection zone are the same in the photosphere. We calculate individual diffusion time-scales for each element (column 3 of Table 2) using the techniques described in Koester (2009)⁴, taking the total mass of helium in the convection zone to be $M(\text{He})_{\text{cvz}} = 2.605 \times 10^{-9} M_{\odot}$. The accretion rates of each element onto the white dwarf are then proportional to the ratio of the the photospheric metal abundance to the diffusion time-scale, leading to the results in column 4 of Table 2.

The accretion/diffusion computations of Koester (2009) assume that accretion has been ongoing for $\gtrsim 5$ diffusion time-scales, reaching a steady-state between material diffusing out of the convection zone and accreting onto the white dwarf. This assumption is likely valid as a dusty debris disc is detected (Brinkworth et al. 2012), which is almost certainly the source of the metals. Girven et al. (2012) showed that such discs have an estimated lifetime of several 10^5 yr. As the diffusion time-scales are only of order 10^4 yr it is reasonable to assume that a steady-state has been reached.

However, we cannot exclude the possibilities that the debris disc formed recently and that accretion and diffusion have not reached a steady-state (the early-phase), or that the accretion rate may not be constant over sufficiently long time-scales. The presence of a gaseous component to the debris disc (§5) has been suggested to be the result of dynamical activity in the disc (Veras et al. 2014a), which may affect the accretion rate. As the lifetime of the gaseous component is likely to be short relative to the diffusion time-scale (Wilson et al. 2014), its presence may be a sign of recent changes in the accretion rate. In this case, known as the instantaneous assumption, the relative chemical abundances in the accreted material will match the photospheric

⁴ See updated values at <http://www1.astrophysik.uni-kiel.de/~koester/astroph>

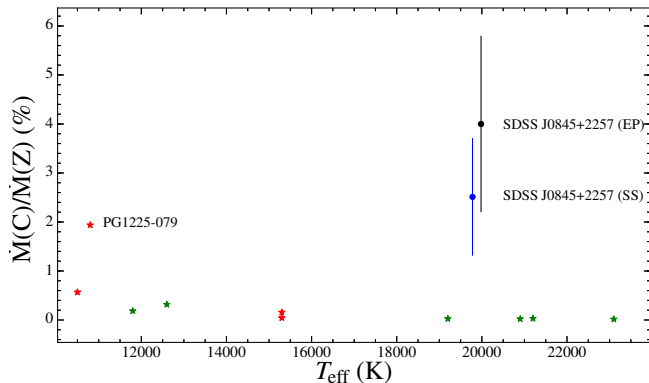


Figure 8. Mass fraction of carbon in the accreted material analysed in the most heavily polluted white dwarfs (Zuckerman et al. 2011; Klein et al. 2011; Dufour et al. 2012; Gänsicke et al. 2012; Farihi et al. 2013; Xu et al. 2013, 2014). Both the early-phase (black) and steady-state (blue) results for SDSS J0845+2257 are shown, with the marker for the early-phase offset by +200 K for clarity. Whilst the carbon fraction is low and roughly constant for both DA (green star symbols) and DB (red star symbols) white dwarfs regardless of T_{eff} , there are two clear outliers: PG 1225-079 (Xu et al. 2013) and SDSS J0845+2257.

abundances. Jura et al. (2015) based their analysis of the debris composition on the instantaneous assumption, as at the $T_{\text{eff}} = 18700$ K used in their analysis the diffusion time-scales are much longer, making it much less likely for the accretion to have reached a steady-state.

Table 3 shows the relative mass fractions of the elements under both the steady-state and early-phase/instantaneous scenarios. We find that the choice of accretion scenario has only a small effect on the elemental mass fractions, with the possible exceptions of C and Ni. Our discussion below of the debris composition is based on the steady-state assumption, but we note where the differences between steady-state and early-phase accretion are significant.

4.1 Total Accretion Rate and Mass of the Parent Body

At $1.6 \times 10^{10} \text{ g s}^{-1}$, SDSS J0845+2257 has one of the highest inferred accretion rates detected at a metal-polluted white dwarf, with the observed elements representing the bulk of those making up the Earth (Table 3). Any additional undetected elements make up only trace amounts, so we can therefore draw reliable conclusions about the bulk abundances of the accreted material.

The total mass of metals calculated to be in the convection zone is $4.9 \times 10^{21} \text{ g}$, setting a lower limit on the mass of the accreted object (or objects). Assuming a rock-like density of $\rho \approx 2\text{--}4 \text{ g cm}^{-3}$, the mass is equivalent to a spherical object with a $\sim 130\text{--}170$ km diameter. However, detection of circumstellar gas (Gänsicke et al. 2008) and dust (Brinkworth et al. 2012) implies that accretion is still ongoing. If a large proportion of the debris is still in the disc, and/or has already sunk out of the convection zone of the white dwarf, then the total mass of the progenitor object may have been significantly higher than that currently present in the convection zone.

4.2 Carbon

Figure 8 shows that the mass fraction of carbon in the accreted material for nearly all of the most heavily polluted white dwarfs is $\lesssim 0.5$ percent, regardless of temperature, for both hydrogen (DA) and helium (DB) atmospheres. However two DB white dwarfs, PG 1225-079 (Xu et al. 2013) and SDSS J0845+2257, have much higher carbon abundances. In PG 1225-079, which has a carbon mass fraction of 1.9 percent, Xu et al. (2013) found no exact match of any solar system object and suggested that the accretion may have been caused by two or more objects with different compositions. Jura et al. (2015) found a carbon mass fraction of 15 percent in SDSS J0845+2257, which, assuming that all of the carbon was accreted, is consistent with that of Interplanetary Dust Particles (IDPs). As IDPs are too small to make up the high inferred accretion rate, Jura et al. (2015) suggested that the disrupted rocky body was a Kuiper-belt analogue which lost its water content during the post main-sequence evolution of the system. Although our diffusion calculations still return an unusually high carbon abundance (2.5 percent in steady-state, 4.0 percent in early-phase), it is significantly lower than that found by Jura et al. (2015) and thus does not match the abundances found in IDPs. The large discrepancy between the carbon mass fractions derived from the two studies arises from the combination of a lower photospheric abundance of carbon determined from our COS ultraviolet spectroscopy (§ 3) and a systematically higher abundance of heavier elements. However, although the detailed results of the two studies differ, the fundamental conclusion of an unusually large abundance of carbon in the photosphere of SDSS J0845+2257, when compared to other debris-polluted white dwarfs, remains. We consider several alternative possible explanations for the excess carbon.

Firstly, Veras et al. (2014b) speculated that a small fraction of the debris at white dwarfs could be made up of exo-Oort cloud comets, which do have a substantial carbon fraction (Jessberger et al. 1988). However, comets have a much higher water content than that observed here (§ 4.3) and cannot supply enough mass to explain the high rate and total amount of accreted metals.

Another scenario that could explain the high carbon abundance in SDSS J0845+2257 is based on results from terrestrial seismology, which have shown that a portion of the Earth’s core must be made up of less dense material than the majority Fe and Ni (Allègre et al. 1995). Carbon has been suggested as a possible candidate for this material (Poirier 1994; Zhang & Yin 2012). The enhanced levels of known core elements (Table 3, § 4.5) at SDSS J0845+2257 could therefore explain the increased carbon abundance. However, the similarly enhanced level of core material detected in PG 0843+516 (Gänsicke et al. 2012) was not accompanied by an increase in the carbon mass fraction.

An alternative explanation is that the carbon present in the atmosphere of SDSS J0845+2257 has not been accreted from planetary debris, but is instead primordial to the white dwarf. A number of DB white dwarfs have been observed with atmospheric pollution from carbon, but no other metals (Provencal et al. 2000; Koester et al. 2014b). These white dwarfs span a range of T_{eff} and no single explanation (in the absence of accretion) can currently explain

the high carbon abundances. At temperatures $\lesssim 16000$ K convection can dredge up carbon from the core into the helium layer (Koester et al. 1982), although some DBs have been observed with carbon abundances much lower than predicted by this model (Desharnais et al. 2008). We note that the maximum contamination by dredge-up is thought to occur near 12000 K (Pelletier et al. 1986), providing an entirely plausible source for the carbon detected in PG 1225-079 ($T_{\text{eff}} = 10800$ K, Xu et al. 2013). The carbon in hotter (>20000 K) white dwarfs, which cannot be explained by the classical dredge up model, has been postulated to be raised by a weak stellar wind (Fontaine & Brassard 2005), but there is currently no working model for the necessary wind acceleration. Both the dredge-up and stellar wind models predict a very low carbon abundance in the temperature range ~ 17000 – 20000 K.

However, the efficiency of photospheric carbon pollution by dredge-up depends not only on the depth of the convection zone, but also on the total mass of the helium layer (Weidemann & Koester 1995). The bulk of the DQ white dwarfs can be modelled with helium envelopes of $\simeq 10^{-3}$ – $10^{-2} M_{\odot}$ (e.g. Fontaine & Brassard 2005), which is in agreement with the helium masses predicted by stellar evolution models (e.g. Lawlor & MacDonald 2006). However, a number of DB white dwarfs (Koester et al. 2014b), cooler DQ (Dufour et al. 2005; Koester & Knist 2006), as well as the recently discovered hot DQ white dwarfs (Dufour et al. 2007, 2008) have higher carbon abundances than predicted by the canonical dredge-up scenario, which can be explained with thinner helium layers (Althaus et al. 2009; Koester et al. 2014b). Assuming that the unusually high carbon abundances in SDSS J0845+2257 are a result of dredge-up would require a thin ($\log(M_{\text{He}}/M_{\text{wd}}) \sim -4.6$) helium layer. In the light of the ongoing discussion of carbon abundances in helium atmosphere white dwarfs, and in the absence of a robust sample of helium layer measurements for white dwarfs, we conclude that dredge-up is a plausible origin of the photospheric carbon in SDSS J0845+2257.

An independent evaluation of the origin of the atmospheric carbon may be provided by the models of Hartmann et al. (2014), which predict that even a relatively small mass fraction of carbon ($>10^{-4}$) in the circumstellar debris should lead to emission from gaseous C II at 8683 Å and 8697 Å. Given that we do detect emission from gaseous Ca II (§5), the non-detection of C II could be further evidence that the carbon is primordial to the white dwarf. Hartmann et al. (2011) applied the same model to the gaseous disc around SDSS J1228+1040, again finding that the absence of C II 8683 Å and 8697 Å emission features in spectra obtained by Gänsicke et al. (2006) requires a low ($\lesssim 0.5$ percent) carbon mass fraction in the gas. Gänsicke et al. (2012) showed that SDSS J1228+1040 has an extremely low photospheric carbon abundance, unambiguously demonstrating that the debris disc in this system is indeed strongly carbon-depleted.

4.3 Oxygen

Measurements of the oxygen abundance in the accreting white dwarf GD 61 by Farihi et al. (2013) suggested that a large fraction of the debris was made of water. To estimate the water content in the debris around SDSS J0845+2257 we

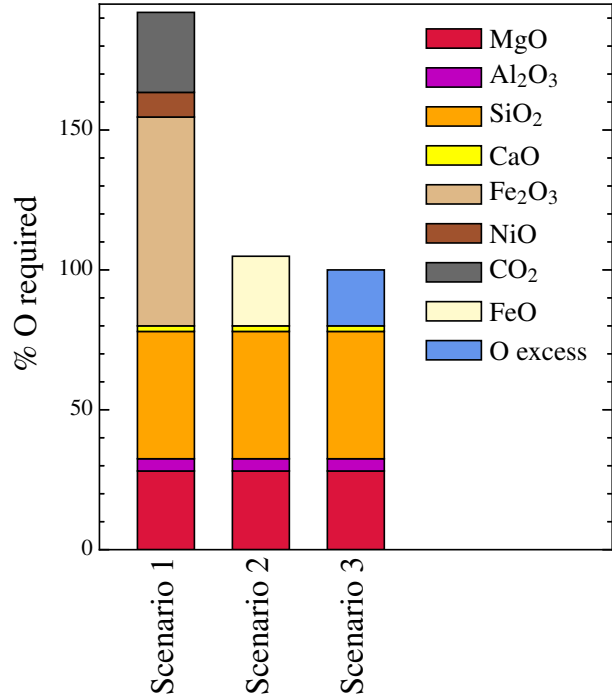


Figure 9. Oxygen budgets of the debris at SDSS J0845+2257, with three scenarios for different contributions of oxygen carriers: 1. All Fe as Fe_2O_3 , CO_2 and NiO present; 2. 50 % of Fe as FeO; 3. All Fe is metallic, making no contribution to the O budget. The third model is the only one to produce a marginal oxygen excess, suggesting that very little water was present in the parent body.

follow the procedure of Farihi et al. (2013), assessing first oxygen carriers other than water. We assume that all of the accreting Mg, Al, Si, and Ca is bound into MgO , Al_2O_3 , SiO_2 and CaO . If the debris is a fragment of a differentiated object then the Fe and Ni content may be split into oxides from the mantle and metallic Fe and Ni from the core, so we present three scenarios for the remaining elements: 1. A conservative scenario where all of the Fe is bound into Fe_2O_3 , Ni into NiO and C into CO_2 ; 2. An intermediate scenario where C is primordial (see §4.2), the contribution from Ni is negligible and half the Fe is present as FeO; 3. A mantle depleted scenario, discussed further in §4.5, where there is no contribution from Fe, Ni or C. Only the third of these scenarios produces an oxygen excess, indicating that the accreted material was likely very dry regardless of the relative contributions from mantle and core material, as well as from carbon. This result is consistent with the low H abundance detected in the atmosphere (Table 2), and is not significantly altered under the assumption of early-phase or instantaneous accretion. Scenario 1 shows that there is insufficient oxygen to account for all of the potential carriers, an indicator that a large fraction of the Fe in the progenitor object was indeed metallic.

4.4 Refractory Lithophiles

Figure 10 compares the abundance of Ca and Al with respect to Si. These elements are two of the main refractory lithophiles: elements which sublime only at very high temperatures and are therefore found mainly in the mantle and

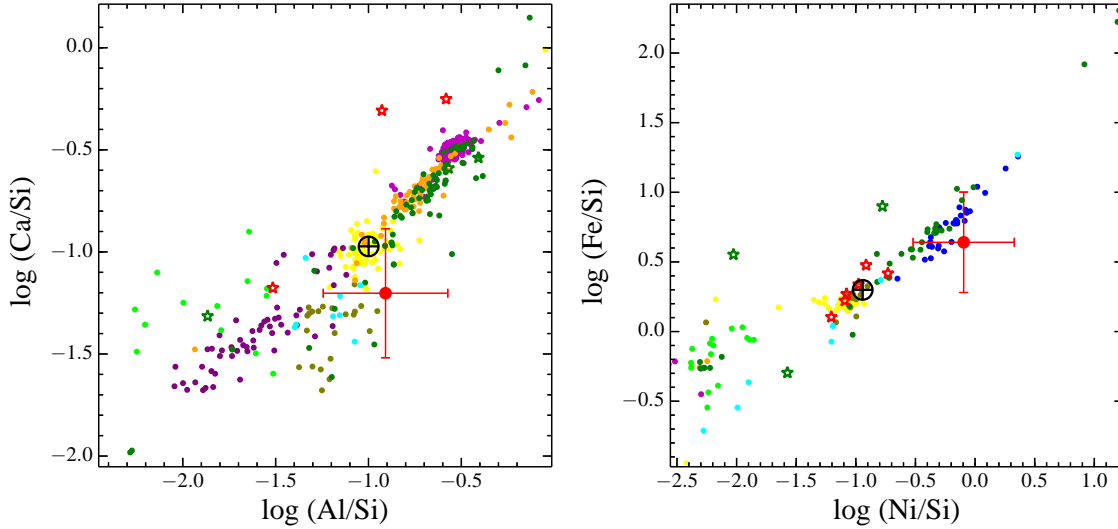


Figure 10. Comparison of the abundance of Al and Ca (left) and Fe and Ni (right) in SDSS J0845+2257 (red marker) with the bulk Earth (\oplus) (McDonough 2000) and the allasite (blue), mesosiderite (dark green), IAB (cyan), urelite (light green), ordinary chondrite and carbonaceous chondrite (yellow), enstatite chondrite (green-brown), Howardite (orange), Eucrite (magenta) and Diogenite (purple) meteorites (Nittler et al. 2004). The most heavily metal-polluted white dwarfs are plotted as green (DAZ) and red (DBZ) stars (Zuckerman et al. 2011; Klein et al. 2011; Dufour et al. 2012; Gänsicke et al. 2012; Xu et al. 2014, 2013; Farihi et al. 2013; Xu et al. 2014). All abundances are normalised to Si.

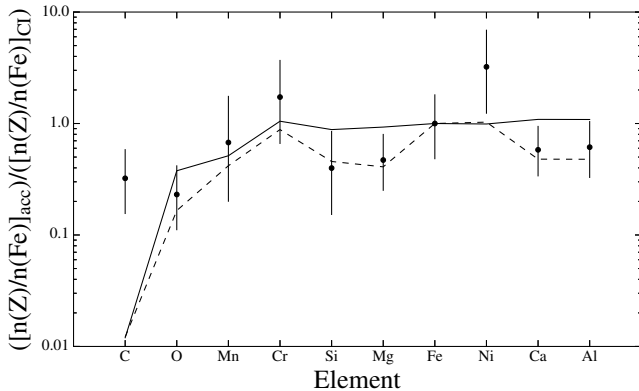


Figure 11. Elemental abundances of the accretion onto SDSS J0845+2257 relative to the abundance in CI chondrites, both normalised to Fe (black dots). The condensation temperature of the elements increases to the right. The solid line shows the abundances of the bulk Earth, whilst the dotted line shows a ‘wind stripped’ model (Melis et al. 2011) in which approximately 15 percent of the silicate Earth has been removed.

crust of differentiated objects (Grossman 1972). The ratio of these two elements is nearly constant in most solar system bodies, such that there is a linear correlation between Ca/Si and Al/Si. The Ca and Al accreting onto SDSS J0845+2257, as well as onto the other heavily polluted white dwarfs, also falls onto or near this line. This indicates that similar geochemical processes are taking place in these systems, and strengthens the case that analysing the accreted debris in the white dwarf photosphere provides a reliable representation of the chemical composition of a terrestrial object at SDSS J0845+2257.

4.5 Iron and Nickel

Table 3 shows that the dominant element in the debris at SDSS J0845+2257 is Fe, with a mass fraction of 40.8 percent, substantially higher than in the Earth. Ni, which is the other major component in the Earth’s core (McDonough 2000), is also enhanced relative to the Earth. Figure 10 shows the linear relationship between Fe/Si and Ni/Si found in the solar system bodies. Whilst the heavily polluted DB white dwarfs also fall on this line, the DA white dwarfs are less confined. SDSS J0845+2257 is close to the trend but has a higher Ni/Fe ratio (≈ 0.2) than the Earth (0.06). In the early-phase model the Ni/Fe ratio drops to ≈ 0.09 .

The high Fe and Ni abundances suggest that the progenitor of the debris at SDSS J0845+2257 may have been a fragment of a larger, differentiated planetesimal with a relatively large core. This could be evidence that some of the processes thought to be responsible for Mercury’s large core, such as partial volatilization (Cameron 1985) or iron/silicate fractionation (Weidenschilling 1978), also occur in extrasolar planetary systems. However, it is likely that any planet close enough to its star for these processes to occur would have been engulfed during the red giant phase, unless it migrated outwards after formation.

Melis et al. (2011) proposed an alternative model in which a planetesimal is eroded by the intense stellar wind during the asymptotic giant branch (AGB). Figure 11 shows this model applied to SDSS J0845+2257. Following the technique detailed in Melis et al. (2011), we show the abundances of the material accreted onto the white dwarf (Table 2) relative to the abundances in the CI chondrites (Lodders 2003), both of which are normalised to Fe. Combining the abundances for the core and silicate Earth from McDonough (2000) we normalise the abundances in the bulk Earth in the same way (solid black line). We then remove $\sim 15\%$ of the

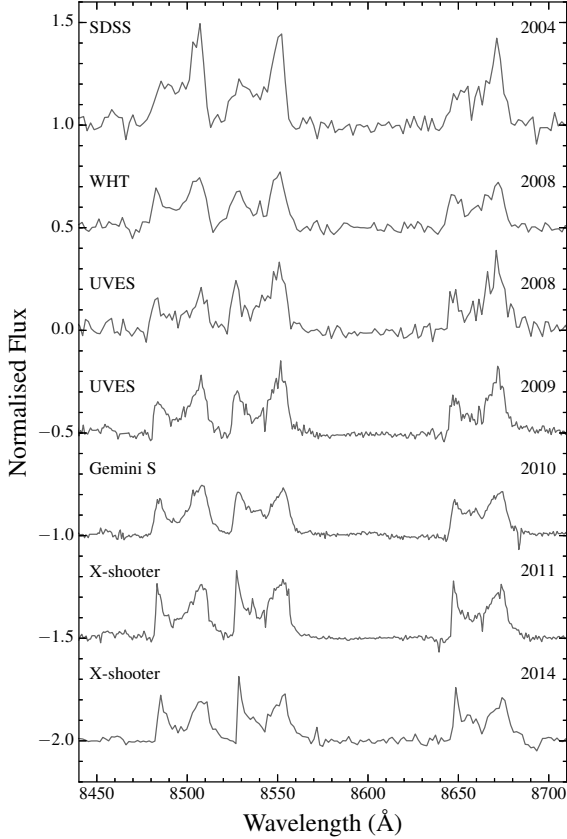


Figure 12. Time-series spectra of the Ca II 8600 Å emission line triplet, plotted on the same scale with each successive spectrum offset by -0.5. The SDSS data from 2004 show a pronounced asymmetry between the two peaks, with the red peak significantly greater in strength. This difference has since vanished, although in the most recent two spectra the blue peak appears marginally stronger.

silicate material (dotted line in Figure 11), simulating the erosion of the mantle of a terrestrial object by stellar wind. We neglect any contribution from the crust, as it makes up only ≈ 0.5 percent of the silicate Earth (Allègre et al. 1995). As can be seen in Figure 11 the dominant elements of both Earth and SDSS J0845+2257 (e.g. Si, O, Mg, Ca, Al) appear to support this model, whilst the trace elements (Mn, Cr) are consistent with both scenarios. The high abundances of C (if accreted, see § 4.2) and Ni remain unexplained, although Ni does become consistent with the model under the early-phase assumption. We note that, whilst Jura (2008) explored the effects of stellar winds on small asteroids, no detailed modelling has been done for the stripping of larger objects and it is unclear if the stellar wind during the AGB can provide the level of erosion suggested here and in Melis et al. (2011).

5 VARIABILITY OF THE CA II TRIPLET

SDSS J0845+2257 is part of a rare subset of metal-polluted white dwarfs that show double-peaked emission in the 8600 Å Ca II triplet, indicative of a gaseous component to the debris disc (Gänsicke et al. 2006, 2007, 2008; Gänsicke 2011;

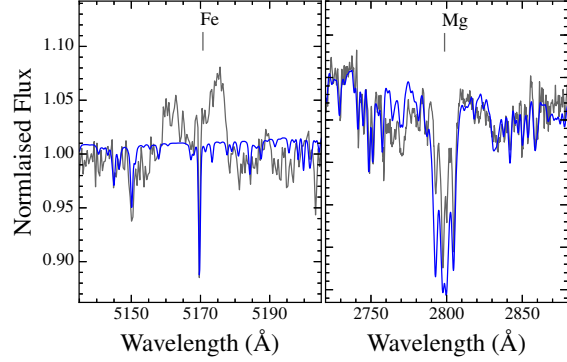


Figure 13. Left: Example of weak double-peaked emission from Fe II. Right: The emission from Mg II predicted by Hartmann et al. (2014) is not detected, but could be masked by the photospheric absorption lines. The model atmosphere fit (blue) over-predicts the strength of the Mg II absorption, which could be due to some flux contribution by emission from the gaseous disc.

Table 4. Change in the equivalent width of the Ca II 8600 Å emission line triplet. The strength of the triplet dropped in the period 2004–2008, but has remained stable to within 1σ since.

Date	Ca II 8600 Å Equivalent Width (Å)
2004 December 19	-16.9 ± 2.2
2008 January 02	-10.3 ± 1.3
2008 April 03	-10.8 ± 1.4
2009 April 10	-11.4 ± 1.4
2010 April 02	-10.5 ± 1.3
2011 January 29	-12.8 ± 1.5
2014 October 20	-8.6 ± 1.1

Melis et al. 2012; Farihi et al. 2012; Wilson et al. 2014). The formation and evolution of these gaseous discs is still poorly understood, as the gas resides outside of the sublimation radius, within which gas is naturally expected to be present, and they are found at only a small fraction of the white dwarfs with dusty discs. There is no known case of a purely gaseous disc.

Time-series observations of the 8600 Å Ca II triplet are shown in Figure 12. The double-peaked morphology arises from the Doppler shifts induced by the Keplerian velocity of the material in the disc (Horne & Marsh 1986), a consequence of which is that the inner and outer radii of the disc can be estimated from the total width and peak separation of the Ca II lines respectively. We find $R_{\text{in}} \sin^2 i \approx 0.3 R_{\odot}$ and $R_{\text{out}} \sin^2 i \approx 0.8 R_{\odot}$, (where i is the unknown inclination of the disc), consistent with the measurements of Gänsicke et al. (2008). Modelling the observed infrared excess, Brinkworth et al. (2012) estimated the extent of the dusty disc to extend from $R_{\text{in}} \approx 0.17 R_{\odot}$ to $R_{\text{out}} \approx 99.7 R_{\odot}$, although the outer radius of the disc is unconstrained due to the lack of observations at longer wavelengths. The overlap of these values strongly suggests that the gaseous and dusty components are co-orbital. Hartmann et al. (2014) attempted to better constrain the parameters of the gaseous disc component using a non-LTE spectral model, but were unable to obtain a satisfactory fit to the emission lines.

The debris discs have provided some of the clearest

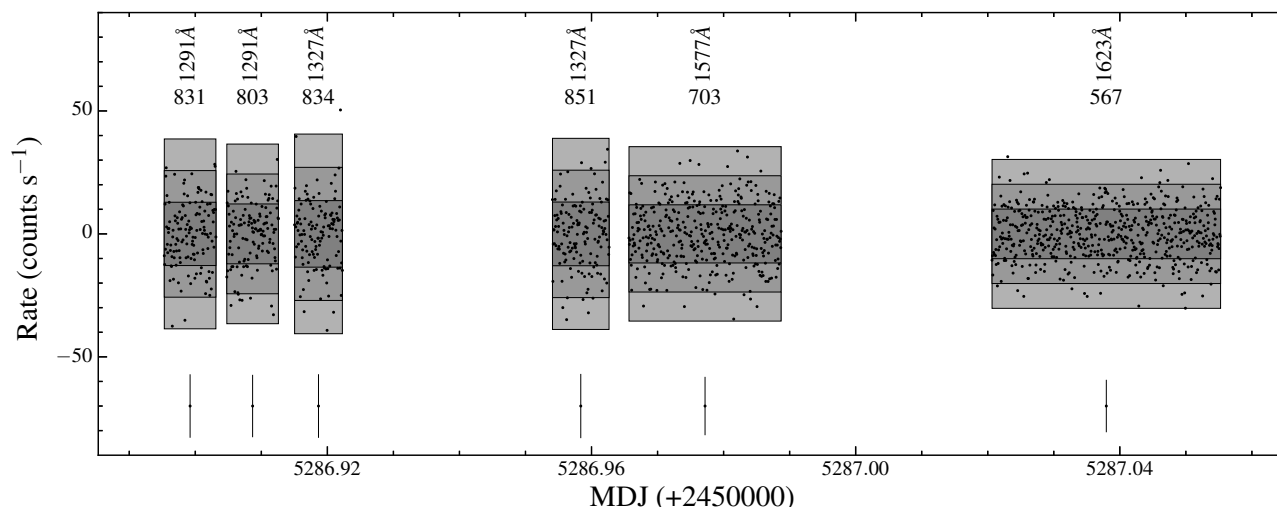


Figure 14. Background-subtracted, normalised light curves of SDSS J0845+2257, extracted from the *HST*/COS time-tag data. Dark grey, grey and light grey areas represent $1\text{-}\sigma$, $2\text{-}\sigma$ and $3\text{-}\sigma$ standard deviations from the mean respectively, assuming a normal distribution for the count rate in each observation. The vertical and horizontal numbers above each spectrum are the central wavelength and mean count rate, respectively. An error bar showing the typical photon noise is shown beneath each spectrum.

evidence for variability in evolved planetary systems, in particular the rapid appearance and loss of the gaseous disc around SDSS J1617+1620 (Wilson et al. 2014) and the drop in infrared luminosity from the dust at WD J0959–0200 (Xu & Jura 2014). Similar, although less pronounced, changes are observed in the 8600 Å Ca II emission line triplet of SDSS J0845+2257. Table 4 lists the change in equivalent widths of the Ca II emission lines over time. The equivalent width was calculated over all three double peaked lines to avoid systematic uncertainties caused by the overlap between the 8495 Å and 8542 Å components. The main source of uncertainty in the measurement is the polynomial fit used to normalise the spectrum. To account for this the fit was varied slightly and the resulting scatter in the equivalent width measurements incorporated into the stated error. The data demonstrate a $\approx 1/3$ drop in the equivalent width of the emission lines between 2004 and 2008, but the strength of the lines has remained constant to within 1σ since then. In addition, the time-series spectra (Figure 12) show pronounced changes in the morphology of the lines. In the 2004 SDSS observation in the red-shifted peaks were substantially stronger, but in more recent observations they have decreased in strength. Conversely the blue-shifted peaks have grown, to the extent that they have become slightly stronger than the red peaks in the latest observations. Due to the relatively low cadence of the time-series observations compared with SDSS J1617+1620 (Wilson et al. 2014) we can only speculate about the cause of this variability, e.g the interaction with a debris stream formed by a tidally disrupted planetesimal (see for example Debes et al. 2012; Veras et al. 2014a).

In addition to the Ca II emission line triplet, some of our spectra show double-peaked emission around the Fe II 5170 Å line (Figure 13, left panel). The Fe II emission is weaker and less variable than the emission from Ca II, with an average equivalent width of -0.8 ± 0.5 Å. Hartmann et al. (2011) predicted emission from the gaseous disc from 2797 Å Mg II, and detected it in the *HST* spectrum of SDSS J1228+1040. We

do not detect emission from Mg II in SDSS J0845+2257 (Figure 13), although the observed Mg II absorption line triplet is weaker than predicted by the model atmosphere fit, possibly due to a small flux contribution from a disc emission line.

It is intriguing that the three white dwarfs with the highest and third highest inferred accretion rates, SDSS J0738+1835 (Dufour et al. 2012) and SDSS J0845+2257 respectively, both host debris discs with gaseous components. Unfortunately, measurements of the total metal accretion rate have only been made for five gas-hosting white dwarfs to date⁵, so the sample size is too small to reliably test any correlation between the presence of gas and the accretion rate.

6 SHORT TERM VARIABILITY

We used the time-tag *HST*/COS photon event files to construct a light curve. To perform the background subtraction for each of the six individual G130M/G160M observations we defined two regions on the COS detector, one below and one above the spectrum. The 1200 Å Ni I, 1216 Å Lyman α and 1302 Å O I airglow emission lines were masked and the edges of the detector segments excluded to reduce the instrumental noise. Figure 14 shows a background-subtracted, normalised light curve binned to 5 seconds.

To probe for any variability in the flux from SDSS J0845+2257 caused by ongoing metal accretion we used a χ^2 test, constructing a light curve using a bin size of 32 ms, i.e. the intrinsic time resolution of COS in time-tag mode. The box for the extraction of the spectrum was defined so that all counts of the target were included, while

⁵ SDSS J0738+1835 (Dufour et al. 2012), SDSS J1228+1040 (Gänsicke et al. 2012), He 1349-2305 (Melis et al. 2012), SDSS J1617+1620 (Wilson et al. 2014) and SDSS J0845+2257 (this work).

minimising the amount of background contribution. We set our null hypothesis that each light curve chunk is constant at the mean value. We find that a constant light curve has an 8–90 percent probability of having the observed distribution, meaning that we can not reject the hypothesis that the light curve is constant. The large range in probability is caused by the different total exposure times of the individual light curve chunks.

To confirm this result and investigate any contribution to the variability from the background we repeated the process, this time with a wider box for extracting the spectrum to incorporate more background counts, as well as an identical test across the whole light curve. The difference in the results is not significant, so we conclude that the *HST*/COS data does not show significant variability on time-scales of 32 ms to \simeq 30 minutes.

As is obvious from Figure 14, no transits by planets or planetesimals are detected. This non-detection is unsurprising, due to both the short duration of the observations and the fact that close-in planets around white dwarfs are probably rare (Veras & Gänsicke 2015).

7 CONCLUSION

We have carried out a detailed spectroscopic study, over a wide wavelength range, of the metal-polluted white dwarf SDSS J0845+2257. The star is accreting debris at a rate of $1.6 \times 10^{10} \text{ g s}^{-1}$ and the mass of metals in the convection zone implies a parent body \gtrsim 100 km in diameter. Measurements of ten metals have shown that the disrupted planetesimal was similar to the Earth in composition, with a differentiated chemistry dominated by O, Mg, Si and Fe. The relatively high levels of Fe and Ni suggests that the planetesimal may have had a portion of its mantle stripped during the AGB phase, leaving a composition dominated by core material. An unusually large amount of carbon is present, although this could be primordial to the white dwarf. The white dwarf is also orbited by a debris disc with a mildly variable gaseous component.

8 ACKNOWLEDGEMENTS

The authors thank M. Jura and the referee, P. Dufour, for constructive discussions regarding the differences in our studies of this object, and C. Manser for performing the telluric correction to the X-shooter spectrum. The research leading to these results has received funding from the European Research Council under the European Union's Seventh Framework Programme (FP/2007-2013) / ERC Grant Agreement n. 320964 (WDTracer). SGP acknowledges financial support from FONDECYT in the form of grant number 3140585.

This paper is based on observations made with the NASA/ESA *Hubble Space Telescope*, obtained at the Space Telescope Science Institute, which is operated by the Association of Universities for Research in Astronomy, Inc., under NASA contract NAS 5-26555. These observations are associated with program ID 11561.

This paper has also made use of observations from the

SDSS-III, funding for which has been provided by the Alfred P. Sloan Foundation, the Participating Institutions, the National Science Foundation, and the U.S. Department of Energy Office of Science.

Observations were also made with the William Herschel Telescope on the island of La Palma by the Isaac Newton Group in the Spanish Observatorio del Roque de los Muchachos of the Instituto de Astrofísica de Canarias, the Gemini South Telescope under program GN-2010A-Q-17, and with the ESO VLT at the La Silla Paranal Observatory under programme IDs 081.C-0466(A), 082.C-0495(A), 383.C-0695(A), 386.C-0218(B) and 094.D-0344(A).

REFERENCES

- Aannestad, P. A., Sion, E. M., 1985, 90, 1832
- Allègre, C., Manhès, G., Lewin, E., 2001, *Earth and Planetary Science Letters*, 185, 49
- Allègre, C. J., Poirier, J., Humler, E., Hofmann, A. W., 1995, *Earth and Planetary Science Letters*, 134, 515
- Althaus, L. G., García-Berro, E., Córscico, A. H., Miller Bertolami, M. M., Romero, A. D., 2009, *ApJ Lett.*, 693, L23
- Barber, S. D., Kilic, M., Brown, W. R., Gianninas, A., 2014, *ApJ*, 786, 77
- Barstow, M. A., Barstow, J. K., Casewell, S. L., Holberg, J. B., Hubeny, I., 2014, *MNRAS*, 440, 1607
- Bergeron, P., et al., 2011, *ApJ*, 737, 28
- Brinkworth, C. S., Gänsicke, B. T., Girven, J. M., Hoard, D. W., Marsh, T. R., Parsons, S. G., Koester, D., 2012, *ApJ*, 750, 86
- Cameron, A. G. W., 1985, *Icarus*, 64, 285
- Casewell, S. L., Dobbie, P. D., Napiwotzki, R., Burleigh, M. R., Barstow, M. A., Jameson, R. F., 2009, *MNRAS*, 395, 1795
- Catalán, S., Isern, J., García-Berro, E., Ribas, I., 2008, *MNRAS*, 387, 1693
- Chayer, P., 2014, *MNRAS*, 437, L95
- Chayer, P., Fontaine, G., Wesemael, F., 1995, *ApJS*, 99, 189
- Chen, Y.-P., Trager, S. C., Peletier, R. F., Lançon, A., Vazdekis, A., Prugniel, P., Silva, D. R., Gonneau, A., 2014, *A&A*, 565, A117
- Debes, J. H., Walsh, K. J., Stark, C., 2012, *ApJ*, 747, 148
- Dekker, H., D’Odorico, S., Kaufer, A., Delabre, B., Kotzlowski, H., 2000, in Iye, M., Moorwood, A. F., eds., *Optical and IR Telescope Instrumentation and Detectors*, vol. 4008 of *Society of Photo-Optical Instrumentation Engineers (SPIE) Conference Series*, p. 534
- Desharnais, S., Wesemael, F., Chayer, P., Kruk, J. W., Saffer, R. A., 2008, *ApJ*, 672, 540
- Dufour, P., Bergeron, P., Fontaine, G., 2005, *ApJ*, 627, 404
- Dufour, P., Liebert, J., Fontaine, G., Behara, N., 2007, *Nat.*, 450, 522
- Dufour, P., Fontaine, G., Liebert, J., Schmidt, G. D., Behara, N., 2008, *ApJ*, 683, 978
- Dufour, P., Kilic, M., Fontaine, G., Bergeron, P., Melis, C., Bochanski, J., 2012, *ApJ*, 749, 6
- Farihi, J., Jura, M., Zuckerman, B., 2009, *ApJ*, 694, 805

- Farihi, J., Gänsicke, B. T., Steele, P. R., Girven, J., Burleigh, M. R., Breedt, E., Koester, D., 2012, *MNRAS*, 421, 1635
- Farihi, J., Gänsicke, B. T., Koester, D., 2013, *Science*, 342, 218
- Fontaine, G., Brassard, P., 2005, in Koester, D., Moehler, S., eds., 14th European Workshop on White Dwarfs, vol. 334 of *Astronomical Society of the Pacific Conference Series*, p. 49
- Gänsicke, B. T., 2011, in Schuh, S., Drechsel, H., Heber, U., eds., *American Institute of Physics Conference Series*, vol. 1331 of *American Institute of Physics Conference Series*, p. 211
- Gänsicke, B. T., Marsh, T. R., Southworth, J., Rebassa-Mansergas, A., 2006, *Science*, 314, 1908
- Gänsicke, B. T., Marsh, T. R., Southworth, J., 2007, *MNRAS*, 380, L35
- Gänsicke, B. T., Koester, D., Marsh, T. R., Rebassa-Mansergas, A., Southworth, J., 2008, *MNRAS*, 391, L103
- Gänsicke, B. T., Koester, D., Farihi, J., Girven, J., Parsons, S. G., Breedt, E., 2012, *MNRAS*, 424, 333
- Genest-Beaulieu, C., Bergeron, P., 2014, *ApJ*, 796, 128
- Gesicki, K., Zijlstra, A. A., Hajduk, M., Szyszka, C., 2014, *A&A*, 566, A48
- Girven, J., Gänsicke, B. T., Steeghs, D., Koester, D., 2011, *MNRAS*, 417, 1210
- Girven, J., Brinkworth, C. S., Farihi, J., Gänsicke, B. T., Hoard, D. W., Marsh, T. R., Koester, D., 2012, *ApJ*, 749, 154
- Graham, J. R., Matthews, K., Neugebauer, G., Soifer, B. T., 1990, *ApJ*, 357, 216
- Green, J. C., et al., 2012, *ApJ*, 744, 60
- Green, R. F., Schmidt, M., Liebert, J., 1986, *ApJS*, 61, 305
- Grossman, L., 1972, *Geochim. Cosmochim. Acta*, 36, 597
- Hartmann, S., Nagel, T., Rauch, T., Werner, K., 2011, *A&A*, 530, A7
- Hartmann, S., Nagel, T., Rauch, T., Werner, K., 2014, *A&A*, 571, A44
- Holberg, J. B., Bergeron, P., 2006, *AJ*, 132, 1221
- Hook, I. M., Jørgensen, I., Allington-Smith, J. R., Davies, R. L., Metcalfe, N., Murowinski, R. G., Crampton, D., 2004, *PASP*, 116, 425
- Horne, K., Marsh, T. R., 1986, *MNRAS*, 218, 761
- Jessberger, E. K., Christoforidis, A., Kissel, J., 1988, *Nat*, 332, 691
- Jura, M., 2003, *ApJ Lett.*, 584, L91
- Jura, M., 2006, *ApJ*, 653, 613
- Jura, M., 2008, *AJ*, 135, 1785
- Jura, M., Xu, S., 2012, *AJ*, 143, 6
- Jura, M., Young, E. D., 2014, *Annual Review of Earth and Planetary Sciences*, 42, 45
- Jura, M., Xu, S., Klein, B., Koester, D., Zuckerman, B., 2012, *ApJ*, 750, 69
- Jura, M., Dufour, P., Xu, S., Zuckerman, B., Klein, B., Young, E. D., Melis, C., 2015, *ApJ*, 799, 109
- Klein, B., Jura, M., Koester, D., Zuckerman, B., 2011, *ApJ*, 741, 64
- Koester, D., 2009, *A&A*, 498, 517
- Koester, D., Knist, S., 2006, *A&A*, 454, 951
- Koester, D., Weidemann, V., Zeidler, E.-M., 1982, *A&A*, 116, 147
- Koester, D., Gänsicke, B. T., Farihi, J., 2014a, *A&A*, 566, A34
- Koester, D., Provencal, J., Gänsicke, B. T., 2014b, 568, A118
- Kowalski, P. M., Saumon, D., 2006, *ApJ Lett.*, 651, L137
- Lawlor, T. M., MacDonald, J., 2006, *MNRAS*, 371, 263
- Lodders, K., 2003, *ApJ*, 591, 1220
- McDonough, W., 2000, in Teisseyre, R., Majewski, E., eds., *Earthquake Thermodynamics and Phase Transformation in the Earth's Interior*, Elsevier Science Academic Press, p. 5
- Melis, C., Farihi, J., Dufour, P., Zuckerman, B., Burgasser, A. J., Bergeron, P., Bochanski, J., Simcoe, R., 2011, *ApJ*, 732, 90
- Melis, C., et al., 2012, *ApJ Lett.*, 751, L4
- Nittler, L. R., McCoy, T. J., Clark, P. E., Murphy, M. E., Trombka, J. I., Jarosewich, E., 2004, *Antarctic Meteorite Research*, 17, 231
- Pelletier, C., Fontaine, G., Wesemael, F., Michaud, G., Wegner, G., 1986, *ApJ*, 307, 242
- Poirier, J.-P., 1994, *Physics of the Earth and Planetary Interiors*, 85, 319
- Provencal, J. L., Shipman, H. L., Thejll, P., Vennes, S., 2000, *ApJ*, 542, 1041
- Raddi, R., Gänsicke, B. T., Koester, D., Farihi, J., Hermes, J. J., Scaringi, S., Breedt, E., Girven, J., 2015, *ArXiv e-prints*
- Rocchetto, M., Farihi, J., Gänsicke, B. T., Bergfors, C., 2014, *ArXiv e-prints no. 1410.6527*
- Saumon, D., Chabrier, G., van Horn, H. M., 1995, 99, 713
- Schlaflly, E. F., Finkbeiner, D. P., 2011, *ApJ*, 737, 103
- Sion, E. M., Aannestad, P. A., Kenyon, S. J., 1988, *ApJ Lett.*, 330, L55
- Steele, P. R., Burleigh, M. R., Dobbie, P. D., Jameson, R. F., Barstow, M. A., Satterthwaite, R. P., 2011, *MNRAS*, 416, 2768
- Tremblay, P.-E., Bergeron, P., Gianninas, A., 2011, *ApJ*, 730, 128
- van Maanen, A., 1917, *PASP*, 29, 258
- Veras, D., Gänsicke, B. T., 2015, *MNRAS*, 447, 1049
- Veras, D., Leinhardt, Z. M., Bonsor, A., Gänsicke, B. T., 2014a, *MNRAS*, 445, 2244
- Veras, D., Shannon, A., Gänsicke, B. T., 2014b, *MNRAS*, 445, 4175
- Vernet, J., et al., 2011, *A&A*, 536, A105
- Weidemann, V., 1960, *ApJ*, 131, 638
- Weidemann, V., Koester, D., 1995, *A&A*, 297, 216
- Weidenschilling, S. J., 1978, *Icarus*, 35, 99
- Wilson, D. J., Gänsicke, B. T., Koester, D., Raddi, R., Breedt, E., Southworth, J., Parsons, S. G., 2014, *MNRAS*, 445, 1878
- Xu, S., Jura, M., 2014, *ApJ Lett.*, 792, L39
- Xu, S., Jura, M., Klein, B., Koester, D., Zuckerman, B., 2013, *ApJ*, 766, 132
- Xu, S., Jura, M., Koester, D., Klein, B., Zuckerman, B., 2014, *ApJ*, 783, 79
- Zhang, Y., Yin, Q.-Z., 2012, *Proceedings of the National Academy of Science*, 109, 19579
- Zuckerman, B., 2014, *ArXiv e-prints no. 1410.2575*
- Zuckerman, B., Becklin, E. E., 1987, *Nat*, 330, 138
- Zuckerman, B., Koester, D., Reid, I. N., Hünsch, M., 2003, *ApJ*, 596, 477

- Zuckerman, B., Koester, D., Melis, C., Hansen, B. M., Jura, M., 2007, ApJ, 671, 872
Zuckerman, B., Melis, C., Klein, B., Koester, D., Jura, M., 2010, ApJ, 722, 725
Zuckerman, B., Koester, D., Dufour, P., Melis, C., Klein, B., Jura, M., 2011, ApJ, 739, 101

This paper has been typeset from a \LaTeX file prepared by the author.